Calculation of the Thermodynamic Solvent Isotope Effect for Ferrous and Ferric Ions in Water

Charles L. Kneifel and Harold L. Friedman
Department of Chemistry, State University of New York, Stony Brook, N.Y. 11794

Marshall D. Newton
Department of Chemistry, Brookhaven National Laboratory, Upton, N.Y., 11973

Z. Naturforsch. **44a**, 385–394 (1989); received February 12, 1989

Dedicated to Professor Jacob Bigeleisen on the occasion of his 70th birthday

Molecular dynamics simulations of molecular models of Fe^{2+} and Fe^{3+} in water ($L_2O = H_2O$ or D_2O) are used to generate various correlation functions that characterize the respective hexaaquo hydration complexes. The static Fe^{2+}-oxygen and Fe^{2+}-hydrogen correlation functions are compared in detail with the first difference neutron diffraction results of Enderby et al. for Ni^{2+}. Velocity autocorrelation functions and corresponding power spectra are generated and analyzed for those modes of hydration shell water molecules whose reduced masses are most sensitive to the changes from H_2O to D_2O. Various approximations are applied to these data to calculate the solvent isotope effect on the difference in hydration free energies for Fe^{2+} and Fe^{3+}. These different approximations all lead to the qualitative conclusion that the net solvent isotope effect reflects a large degree of cancellation between the OL stretching modes and the librational modes. The simulation results generally agree with the results of earlier quantum chemical calculations applied to the same system, but in some respects the new results are not as realistic as the earlier ones. It is proposed that the agreement with experiment would be improved by changes in the model potential which are motivated by other, independent considerations.

1. Introduction

The thermodynamic, spectral, and kinetic properties of aqueous solutes exhibit measurable solvent isotope effects when the solvent is changed from H_2O to D_2O. These phenomena may be dominated by terms due to the effect of a solute particle on the zero-point energies of the adjacent water molecules, as suggested by Bigeleisen [1]. He specifically considered the internal OH stretch modes, while Bernal and Tamm [2] had earlier remarked on the isotope shifts of the librational modes in pure water. In both O–L stretch and librational modes of L_2O (L = H or D) the reduced mass is close to the mass of the L, so there is a large change in frequency and zero-point energy in passing from H_2O to D_2O. This report is one of several [3, 4] in which these qualitative ideas are applied in quantitative detail with the aim of finding whether the measured solvent isotope effect on the ferrous-ferric electron exchange in water is consistent with an outer sphere mechanism for this kinetic process [1, 5].

Reprint requests to Dr. H. L. Friedman, Department of Chemistry, State University of New York, Stony Brook, N.Y. 11794, USA.

Consideration of the experimental data that may be brought to bear on this equation leads to another question [3]: Can one devise a neutron experiment to measure the H/D fractionation between the bulk L_2O and sites in the hexaaquo ions $M(L_2O)_6^{z+}$?

Both questions are related in varying degrees to the measured solvent isotope effect on the solvation free energy, namely the free energy change ΔG_{trans} for the transfer process [6]

$$I(H_2O) \rightarrow I(D_2O). \tag{1.1}$$

It is found that when I is a uninegative anion or a singly or doubly charged metal ion this process exhibits nearly complete entropy-enthalpy compensation [6]. That is, at T near 298 K one finds $\Delta H_{trans} \approx T^* \Delta S_{trans}$ with T^* near 298 K. This sort of compensation, an important feature of many solution phenomena, especially in aqueous solutions [7], has not yet received a quantitative molecular interpretation.

Our earlier studies [3, 4] of these questions were based on the quantum chemical calculation of the z-dependent geometries and frequencies in small complexes [3], $M(H_2O)_6^{z+} \cdot 2\,H_2O$, in which a $M(H_2O)_6^{z+}$ complex is hydrogen-bonded through one water mole-

0932-0784 / 89 / 0500-0385 $ 01.30/0. – Please order a reprint rather than making your own copy.

cule to two others. It was found that major contributions to ΔG_{trans} of M^{z+} come from both the OH stretch and the librational modes of the water molecules. When these terms, which are of opposite sign, approximately cancel then $\Delta G_{\text{trans}} \approx 0$ [6]. On the other hand, the *kinetic* isotope effect on the rate constant for the ferrous-ferric exchange is largely accounted for [4] by the H/D difference in Franck-Condon factors associated with the nuclear tunneling processes involving L_2O. In the kinetic isotope effect the O–L stretch and the libration contributions reinforce each other. They have no tendency to mutually cancel, giving an indication of how there can be a significant kinetic effect even when the thermodynamic effects are relatively small.

Unlike the OH stretch and other intramolecular modes, the librational modes have restoring forces which are entirely *inter*molecular in origin. Such forces are not particularly well represented by interactions within the $M(H_2O)_6^{z+} \cdot 2\,H_2O$ complex, even for that water molecule which is coordinated both to the metal ion and to the two "extra" water molecules. Indeed, some scaling of the quantum-calculated librational frequencies was needed [3]. To calculate the Franck-Condon factors one also needs the effect of changing z upon the equilibrium value of the appropriate librational tunneling coordinate [4], a variable for which it is much more difficult to make a reliable estimate. Therefore we have turned to a molecular dynamics (MD) simulation applied to a model that specifies the water-water and ion-water interactions in order to elucidate some of these questions. To control effects due to unrealistic aspects of the model it is planned to extend this study to other models.

In a recent contribution, Kuharski and Rossky [8] have used a path integral simulation to calculate the quantum effects in H_2O and D_2O. It is possible to extend their method to apply to the present problem but it is estimated that the computing effort for a given model would be at least 100-fold greater than theirs. A contributing factor is the smaller number of data generated by each move (there are 6 L_2O in the metal ion hydration complex, compared to 125 in their basic cell). Even so, while the path integral method would avoid the complications that we encounter in identifying and selecting the vibrational modes, we really need to analyze the overall solvent isotope effect in terms of the contributions from various local modes to get a molecular picture of the thermodynamic solvent isotope effect. When we come to the kinetic solvent isotope effect it is not clear how to effect the path integral option, while the method to calculate contributions from the local modes is already established [4] except for the need to determine the z-dependence of the librational coordinates.

Here we report the portion of our study that is relevant to the solvent isotope effect on the hydration thermodynamics. Further work, in which the Franck-Condon factors are evaluated to estimate the solvent isotope effect upon the kinetics is in course.

2. Molecular Dynamics Simulation

We simulate one M^{z+} ion (Fe^{3+} or Fe^{2+}) in a cubic cell with $N=100$ water molecules, with periodic boundary conditions and approximate Ewald sums [9]. The side length of the cube was 15.56 Å; in the case of Fe^{2+} or Fe^{3+} in H_2O this gives the density (1 g/ml) used by others [10, 11]. On the basis of earlier work by Engstrom et al. [12], concerned with the fluctuating electric field gradients at the nucleus of an ion in water, we expect our MD simulation to be faithful to the dynamics of the $M(H_2O)_6^{z+}$ complex with the assumed model potentials. For models of aqueous Li^+, Na^+, and Cl^-, they [12] found that the hydration shell dynamics was insensitive to changes in boundary conditions for even smaller systems than those considered here.

The modified central force model of Bopp et al. [13] was used for the water-water potential. This model consists of an intermolecular plus an intramolecular potential. The intermolecular potential is a simplified version of a central force model for water [14], while the intramolecular potential is based on the spectroscopic potential of Carney et al. [15].

The following form was used for all I–L_2O (Ion-water) potentials [10]:

$$V_{\text{I}-\text{L}_2\text{O}} = \frac{q_{\text{I}}\,q_{\text{O}}}{r_{\text{IO}}} + \frac{A}{r_{\text{IO}}^2} + B\,e^{-C r_{\text{IO}}} \tag{2.1}$$

$$+ \frac{q_{\text{I}}\,q_{\text{L}}}{r_{\text{IL}_1}} + \frac{D}{r_{\text{IL}_1}^2} + E\,e^{-F r_{\text{IL}_1}} + \frac{q_{\text{I}}\,q_{\text{L}}}{r_{\text{IL}_2}} + \frac{D}{r_{\text{IL}_2}^2} + \text{E}\,\text{e}^{-F r_{\text{IL}_2}}.$$

The parameters for the I–L_2O potentials listed in Table 1 are derived from those of Curtiss et al. [11]. The non-coulombic part of the potential is truncated using a spherical cutoff at half of the box length. In order to avoid discontinuities, a cubic spline function modifies the potentials in the range 7.03 Å $< r <$ 7.28 Å

Table 1. Parameters of (2.2) for V in 10^{-12} erg and r_{ab} in Å.

Ion	A	B	C	D	E	F
Fe^{3+}	−2.689	1989.437	3.626	1.472	0.417	0.699
Fe^{2+}	−6.293	565.447	2.951	3.280	0.770	0.610

Table 2. Static averages from the MD simulation [a].

	Fe^{2+}, H_2O	Fe^{2+}, D_2O	Fe^{3+}, H_2O	Fe^{3+}, D_2O
Run length, ps	38	25	18	12
T/K	323	328	321	315
r_{FeO}/Å [b]	2.15	2.20	2.03	2.05
r_{FeL}/Å [c]	2.89	2.88	2.81	2.81
n_{HS} [d]	6.0	6.0	6.0	6.0
n_{HS} [e]	6.0	6.0	6.0	6.0
r_{OL}	0.99	0.99	1.00	1.00
σ_{FeO} [f]	0.26	0.30	0.24	0.30
σ_{FeD} [f]	0.39	0.52	0.35	0.37

[a] Distances in Ångström units.
[b] Location of First maximum in $g_{FeO}(r)$.
[c] Location of First maximum in $g_{FeL}(r)$.
[d] Coordination number from g_{FeO}.
[e] Coordination number from g_{FeL}.
[f] Linewidth at half height.
The error on all distances is ±0.02 Å except r_{OL} which is ±0.002.

to make the potential and its derivative go smoothly to zero.

MD simultion with the Verlet [16] leapfrog algorithm used a time step of 0.25 fs, small enough to allow us to sample the trajectory of an OH vibration. Each system (see Table 2) was run on a CSPI MAP 6420 attached to a VAX 11/780. A 25 ps run takes approximately 100 CPU hours on the CSPI, equivalent to 800 CPU hours on the VAX.

3. Static Structure

The ion-water radial distribution functions $g_{IO}(r)$ and $g_{IH}(r)$ and the running coordination numbers are shown in Fig. 1 for $I = Fe^{2+}$. The radial distribution functions show sharply defined first peaks which characterize the hydration shell. We calculate the running coordination number of the ion as

$$n(R) = \varrho_O \int_0^R g_{IO}(r)\, d^3r \tag{3.1}$$

or

$$n(R) = \tfrac{1}{2}\varrho_H \int_0^R g_{IH}(r)\, d^3r\,. \tag{3.2}$$

If r_{min} is the location of the minimum of g_{IO} or g_{IH} after the first peak, then $n(r_{min}) \equiv n_{HS}$ is the number of water molecules in the first shell. The relevant data are summarized in Table 2. There is good overall agreement with other simulations [11] in the positions of the first peaks and the shifts between the ferric and ferrous ions. The prominent structural features for $r > 4$ Å reflect the small size of the basic cell. Indeed they are greatly reduced by increasing N from 100 to 200 while keeping the densities (ϱ_O and ϱ_H) and other parameters the same. The structural and dynamical results for the hydration shell in the $N = 200$ simultions are practically the same as those found for $N = 100$, so only the latter are presented.

Enderby et al. have measured the first difference function G_{Ni}, the difference spectrum between two systems with different Ni isotopes, in 1.46 m $NiCl_2$ in D_2O by a neutron diffraction method [17]. The first difference function is a useful probe of hydration shell structure because the water-water structure drops out. We have [17]

$$G_{Ni}(r) = 0.277\, h_{NiO} + 0.637\, h_{NiD} + \ldots, \tag{3.3}$$

where $h_{\alpha\beta} = g_{\alpha\beta} - 1$ and where the missing terms are negligible, as in the present application. It is interesting to compare their result (Fig. 2) with

$$F_{Fe}(r) = 0.277\, h_{FeO} + 0.637\, h_{FeD} \tag{3.4}$$

because we presume that the model Fe^{2+}–O and Fe^{2+}–D potential functions in Sect. 2 would apply almost as well if Fe^{2+} were replaced by Ni^{2+}, the crystal radius [18] of Fe^{2+} (0.91 Å) being scarcely larger than of Ni^{2+} (0.84 Å). (Of course G_{Fe} defined in (3.4) would not apply to a real neutron diffraction experiment on a 1.46 m solution of a Fe^{2+} salt in water because the relevant isotope neutron scattering lengths would differ from those incorporated in (3.4)).

The data in Fig. 2 show only a 0.02 Å shift from the NiO peak to the FeO peak, while there is a 0.20 Å shift from the NiD peak to the FeD peak. These shifts are in the expected direction in view of the different crystal radii.

On the other hand the FeO peak is about 1.7 fold wider (at half height) than the NiO peak while the FeD peak is 1.9 fold wider than the NiD peak. (The linewidth differences are most evident in the peak heights, so the linewidth ratios were actually calculated from the peak heights in view of the fact that the areas under all four peaks fit the stoichiometry of $M(D_2O)_6^{2+}$). In interpreting the linewidth data it must

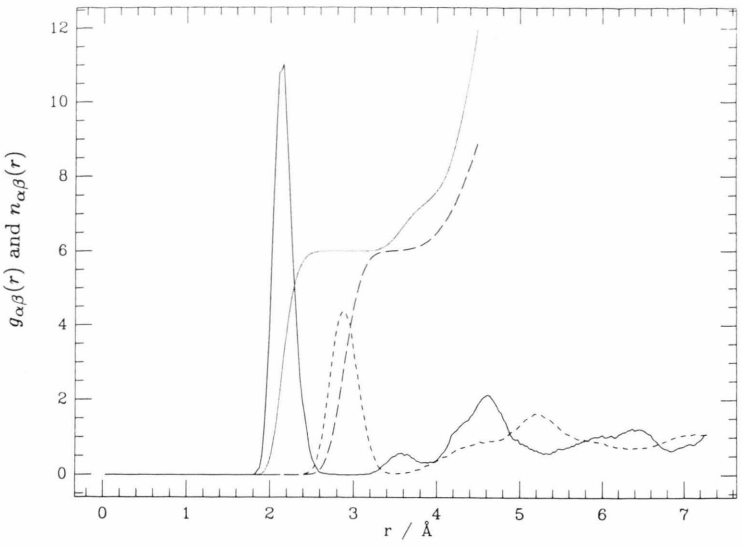

Fig. 1. Typical pair correlation functions $g_{\alpha\beta}(r)$ from the simulation of Fe^{2+} in H_2O (g_{FeO} ——, g_{FeH} – – –, n_{FeO} · · · · ·, n_{FeH} — — —). See Table 2 for the principal results.

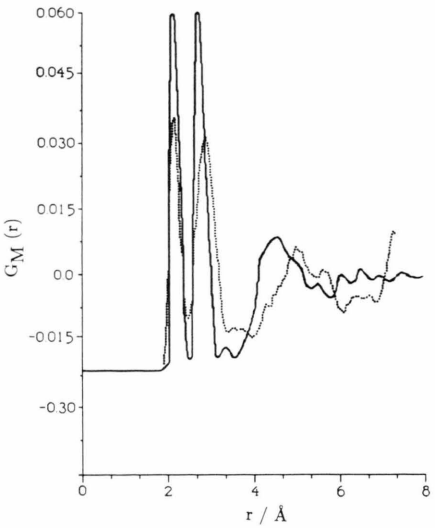

Fig. 2. First order difference neutron diffraction function. Experimental G_{Ni} (——) (cf. (3.3)) for 1.46 *m* $NiCl_2$ in D_2O reported by Enderby and Neilson [17]. G_{Fe}(· · · · ·) given by (3.4). In the figure the ordinate should be labeled 0.0238 D_M.

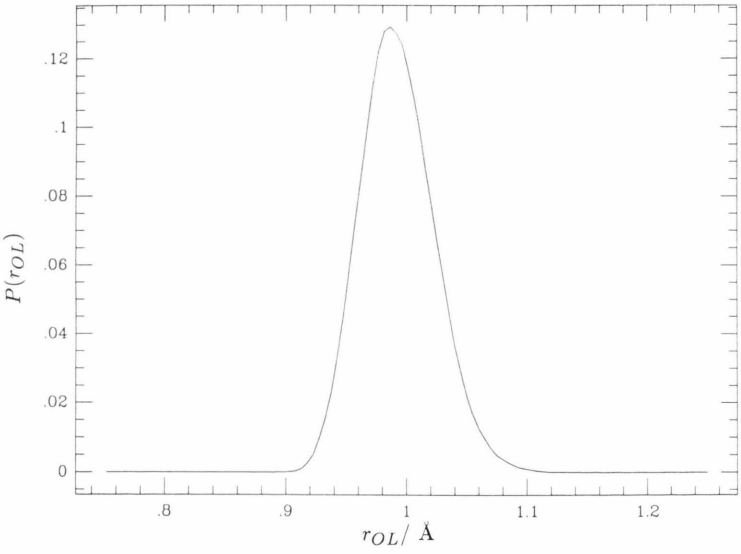

Fig. 3. A typical distribution of r_{OL} distances in the hydration shell; Fe^{2+} in D_2O.

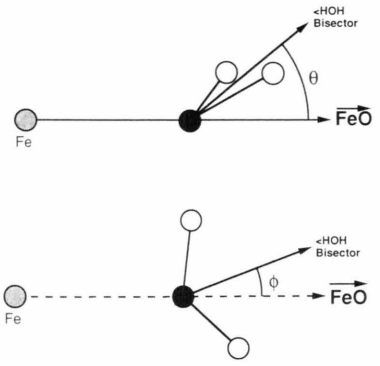

Fig. 4. Definition of angles to specify the orientation of a water molecule (considered as rigid for this purpose) in the field of an Fe^{z+} ion. The solid FeO arrow represents a vector from the Fe^{z+} through the oxygen, while the dashed FeO arrow represents the projection of that vector onto the plane of the water molecule.

be recalled that G_{Ni} is measured at 1.46 *m* while G_{Fe} is calculated from correlation functions derived for infinitely dilute systems. It is unlikely that the linewidth differences noted here are due to concentration differences: the extensive data [17] for G_{Ni} show slight narrowing of the peaks with at most a small shift of the h_{NiD} peak to larger *r* as the concentration is decreased. One conclusion is that the discrepancies between the model FeO and FeD linewidths and what may be expected for the NiO and NiD lines at infinite dilution arise from unrealistic aspects of the model. Some of our simulation results presented below provide a

molecular interpretation of the linewidths in Fig. 2 even though they do not elucidate the differences in linewidths in the Ni^{2+} and Fe^{2+} complexes.

The small peak near 3.3 Å in G_{Ni} in Fig. 2 has sometimes been interpreted as a Ni^{2+}–Cl^- correlation but more recently as due to water molecules outside of the hydration complex [19]. The peak in G_{Fe} near 3.5 Å supports the latter interpretation since G_{Fe} is calculated for a system that has no Cl^- ions.

We calculated the distribution of the O–H bond lengths of the hydration shell water molecules (Fig. 3 and Table 2) for comparison with experimental OH bond lengths, as determined by NMR. The experimental values [20] are $r_{OH}=0.996$ Å in $Mg(H_2O)_6^{2+}$ and $r_{OH}=1.019$ Å in $Al(H_2O)_6^{3+}$. Here is a second indication that our present model is not entirely realistic.

The distributions of two angles (θ and ϕ in Fig. 4) that characterize the orientation of hydration shell water molecules are shown for Fe^{3+} in D_2O in Figure 5. These distributions indicate that the hydration shell water molecules are nearly trigonal (dipole axis towards the metal ion), and thus far from tetrahedral (a lone pair toward the metal ion). We find that a width of 10° in ϕ accounts for a linewidth in $g_{IH}(r)$ of 0.25 Å, whereas a width of 20° in θ gives rise to a linewidth of only 0.04 Å in $g_{IH}(r)$. The ϕ distribution shows that a small deviation from a trigonal configuration can give rise to much larger linewidths than expected if one only considers the distribution of θ (the tilt angle employed in earlier work [17]).

4. Vibrational Modes

The power spectra of various velocity autocorrelation functions are accumulated during the simulation by the method of Futrelle and McGinty [21]. We first consider the power spectra

$$P_X^{L_2O}(\omega)=Re\int_0^\infty dt\langle \boldsymbol{v}_L(t)\cdot\boldsymbol{v}_L(0)\rangle_X e^{-i\omega t} \quad (4.1)$$

of the L atom velocity auto-correlation functions (laboratory frame). In (4.1) the index X denotes either the hydration shell waters (X = HS) or the remaining "bulk" waters (X = B). Thus we have grouped the waters into two separate types as has been done in other simulations [10, 13]. The quantity $\langle \boldsymbol{v}_L(t)\cdot\boldsymbol{v}_L(0)\rangle_X$ denotes an equilibrium ensemble average over the L atoms either in the hydration shell of the cation or in the bulk. The hydration shell phenomena are of primary interest, while, as indicated in Fig. 2, the bulk structure is unrealistic; for these reasons we do not report the bulk water data in detail.

The hydrogen velocity autocorrelation function power spectra can be divided into three distinct regions, which we may characterize in terms of those local modes of the hydration complex in the aqueous medium for which the reduced mass is proportional (or nearly so) to the mass of the L. Referring, for example, to the solution in H_2O (Fig. 6) we see a low frequency region ($0-1000\ cm^{-1}$) corresponding to the librational motions of rigid water molecules. The middle region ($1200-2000\ cm^{-1}$) corresponds to the HOH bending mode. The high frequency region corresponds to the OH stretching modes (symmetric and asymmetric stretching not separated). The OH stretching modes in the hydration shell are red shifted with respect to the bulk while the libration region is blue shifted; thus there is qualitative agreement with the results of Newton and Friedman [3]. The HOH bending mode remains essentially unperturbed by the field from the M^{z+} ion [3].

We now consider the discrete modes associated with hindered rotations about a set of unit vectors ($\hat{Y}$ for yaw, $\hat{P}$ for pitch, and $\hat{R}$ for roll) on each water molecule, as defined in Figure 7. We define them in terms of the oxygen and hydrogen position vectors as follows:

$$\boldsymbol{r}_1=\boldsymbol{r}_{L_1}-\boldsymbol{r}_{cm},\quad \boldsymbol{r}_2=\boldsymbol{r}_{L_2}-\boldsymbol{r}_{cm},\quad \boldsymbol{r}_3=\boldsymbol{r}_O-\boldsymbol{r}_{cm}, \quad (4.2)$$

$$\boldsymbol{Y}=\frac{\boldsymbol{r}_1\times\boldsymbol{r}_2}{|\boldsymbol{r}_1\times\boldsymbol{r}_2|},\quad \boldsymbol{P}=\boldsymbol{R}\times\boldsymbol{Y},\qquad \boldsymbol{R}=\frac{\boldsymbol{r}_1\times\boldsymbol{r}_2}{|\boldsymbol{r}_1\times\boldsymbol{r}_2|}, \quad (4.3)$$

where $\boldsymbol{r}_{cm}$ is the location of the center of mass of the water molecule, and we define the librations as hindered rotations about these vectors:

$$\frac{d\boldsymbol{Y}}{dt}=\boldsymbol{\alpha}_Y\times\boldsymbol{Y}, \quad (4.4)$$

$$\frac{d\boldsymbol{P}}{dt}=\boldsymbol{\alpha}_P\times\boldsymbol{P}, \quad (4.5)$$

$$\frac{d\boldsymbol{R}}{dt}=\boldsymbol{\alpha}_R\times\boldsymbol{R}, \quad (4.6)$$

where $\boldsymbol{\alpha}_m$ is the angular velocity about the m axis. We calculate [21] power spectra for the librational modes from the angular velocity autocorrelation function

$$P_{m,X}^{L_2O}(\omega)=Re\int_0^\infty dt\langle \boldsymbol{\alpha}_m(t)\cdot\boldsymbol{\alpha}_m(0)\rangle_X e^{-i\omega t}. \quad (4.7)$$

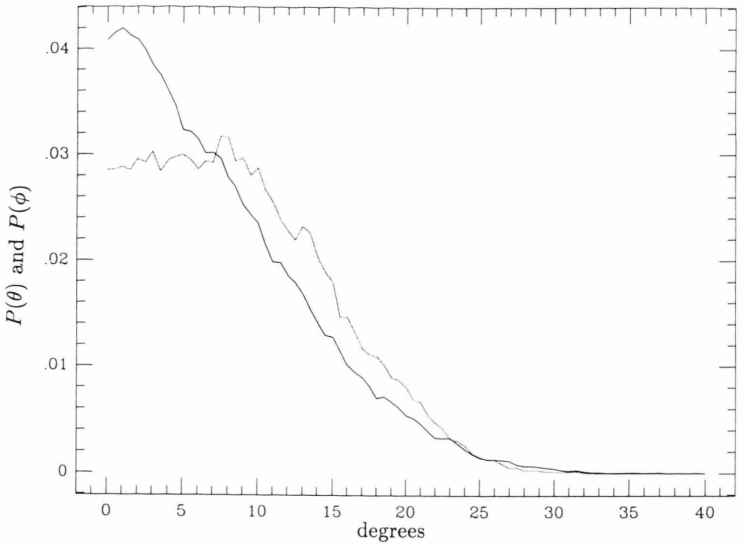

Fig. 5. Distribution of θ (——) and ϕ (· · ·) angles of water molecules in the hydration shell of an Fe^{3+} ion. The first moments of $P(\theta)$ and $P(\phi)$ are 7.7° and 8.9° respectively.

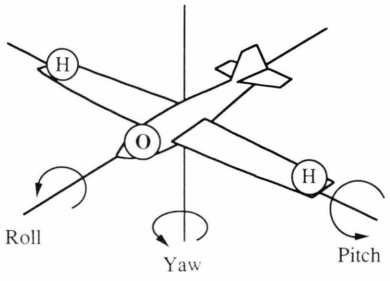

Fig. 7. Definitions of librational modes: roll, pitch, and yaw for a flying water molecule. The relation to the coordinates in Fig. 4 is evident.

Table 3. First moments of the hydration shell vibrational power spectra [a, b]

Solute	Solvent	$\bar{\omega}_{\text{Yaw}}$	$\bar{\omega}_{\text{Pitch}}$	$\bar{\omega}_{\text{Roll}}$	$\bar{\omega}_{\text{Strertch}}$
Fe^{3+}	H_2O	709 ± 8	867 ± 8	577 ± 8	2973 ± 20
Fe^{3+}	D_2O	509 ± 2	619 ± 2	378 ± 8	2195 ± 15
Fe^{2+}	H_2O	650 ± 8	763 ± 8	474 ± 8	3097 ± 20
Fe^{2+}	D_2O	511 ± 2	583 ± 2	369 ± 2	2261 ± 14
Fe^{3+}	D_2O [c]	513 ± 6	649 ± 6	410 ± 6	2173 ± 16
Fe^{2+}	D_2O [c]	470 ± 6	571 ± 6	337 ± 6	2261 ± 12

[a] In units of cm^{-1} at $T \approx 322$ K as calculated from (4.8).
[b] These errors estimates are based on the finite sampling interval in frequency space. The estimated uncertainties due to finite length of trajectories are no larger.
[c] Calculated from the respective H_2O data using (4.9).

We characterize the frequency of the m-th mode by its first moment

$$\bar{\omega}_m = \frac{\int_0^{\omega_{\max}} \omega \, P_{m,X}^{L_2O}(\omega) \, d\omega}{\int_0^{\omega_{\max}} P_{m,X}^{L_2O}(\omega) \, d\omega}, \tag{4.8}$$

where $\omega_{\max}$ is the highest frequency sampled. These frequencies for the hydration shell librational modes, and also for the OL stretching modes (from the hydration shell L atom velocity autocorrelation power spectra (X = HS)), are shown in Table 3. In order to make useful comparison among the different system, all of the first moments in Table 3 were determined for systems at 322 K. This was done by using data for the D_2O system at different temperatures (i.e. from simulations at 301 K and 337 K for Fe^{2+} and 307 K for Fe^{3+}, in addition to those in Table 2) and interpolating the results to 322 K while neglecting the small deviation of the H_2O data from $T = 322$ K. We find that for the librations the blue shifts for the sequence

$$\text{bulk water} \rightarrow \text{water in } Fe(H_2O)_6^{2+} \rightarrow \text{water in } Fe(H_2O)_6^{3+}$$

qualitatively agree with earlier work [3] and with results of Halley and Hautman [22]. Detailed comparison with the latter is difficult due to differences in the model and in the correlation functions calculated.

If each of the local modes discussed above were associated primarily with a single effective normal coordinate of the system, then the power spectrum of each local mode would be dominated by the frequency of the corresponding normal mode. We believe this situation pertains to the hydration complex in H_2O. However in D_2O there are indications of appreciable mixing between the librational modes and the hindered translational modes of the hydration shell waters (i.e., the

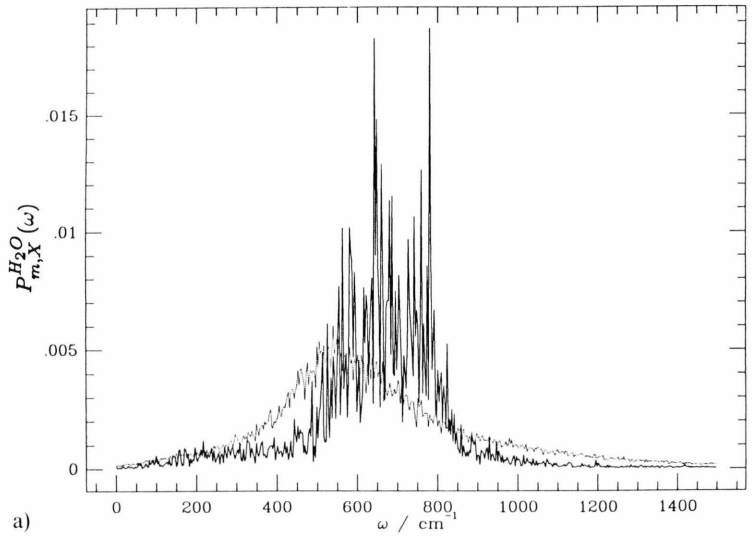

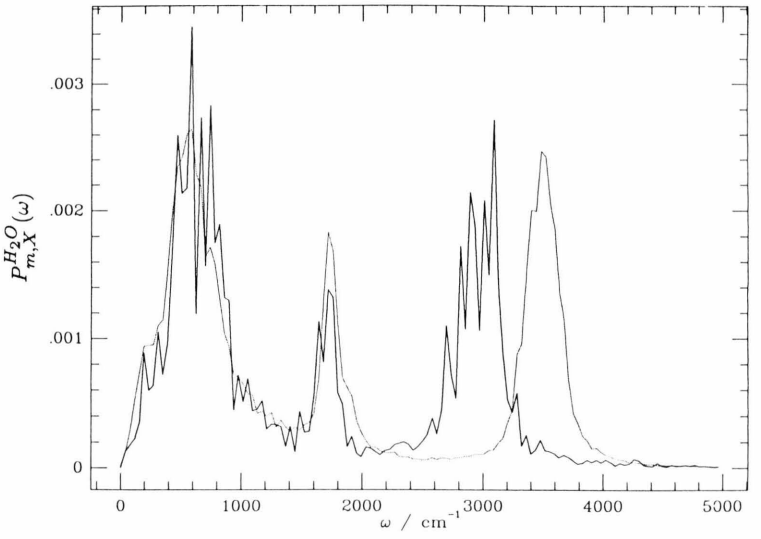

Fig. 6. Velocity autocorrelation function power spectra (bulk · · · · and hydration shell ——) for Fe^{3+} in H_2O.

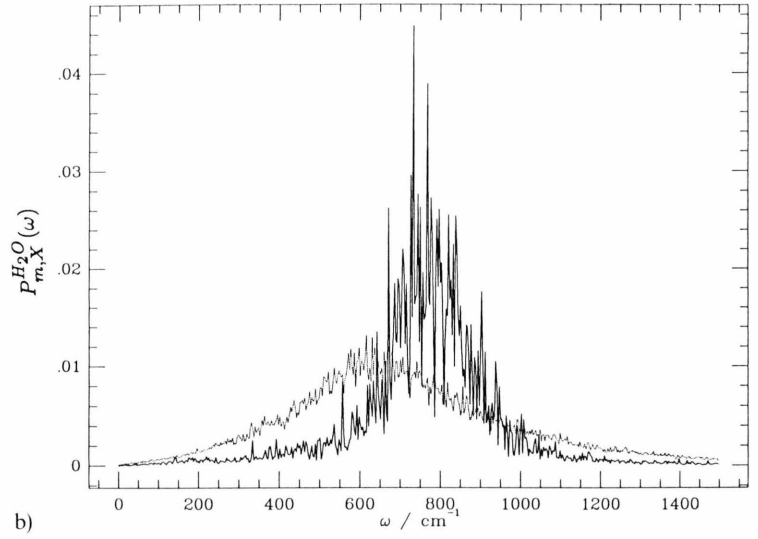

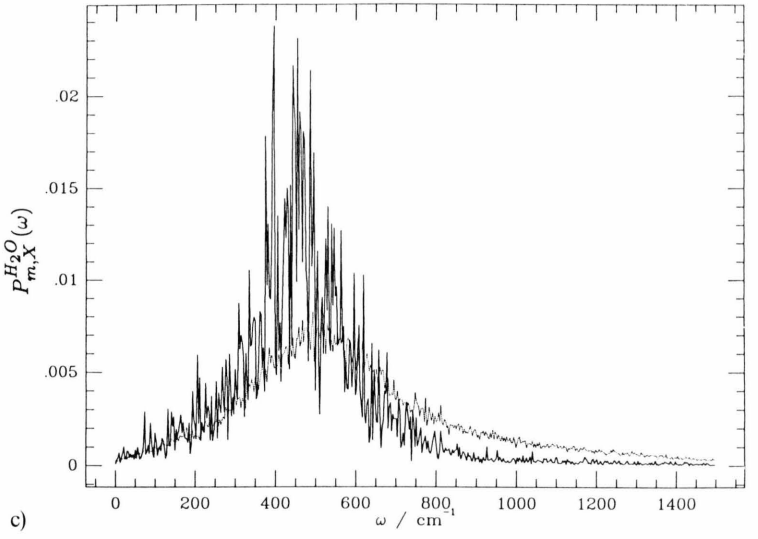

Fig. 8. Power spectra of librational angular velocity autocorrelation functions for Fe^{2+} in H_2O; a) yaw, b) pitch, c) roll (bulk · · · · · and hydration shell ——).

modes of the MW_6 entity, where $M \equiv Fe^{z+}$ and $W \equiv D_2O$ act like point masses) [22, 23]. Hence the power spectra of the local librational modes for D_2O solutions are expected to be more complex than for the corresponding H_2O case; the first moments of the spectra for D_2O solutions represent weighted averages of the normal mode frequencies arising from the mixing of the librational and hindered translational modes. From other studies [22, 23] we find that the hindered translational modes for the hydration shell waters span the frequency range $\approx 200-500\ cm^{-1}$, a range which overlaps with that pertinent to the librational modes of the hydration shell D_2O molecules. The consequence for our purpose is that the librational modes of the hydration shell waters in D_2O can no longer be simply interpreted. As an alternative approach to estimating the frequencies for the local D_2O librational modes, we include $\omega_m(D_2O)$ values derived from the $\omega_m(H_2O)$ results as follows:

$$\omega_m(D_2O) = \sqrt{\frac{I_m^H}{I_m^D}}\ \omega_m(H_2O)\,, \tag{4.9}$$

where I_m^L is the moment of inertia of mode m as derived in the appendix. As shown in Table 3, the D_2O results based on (4.9) are reasonably close to those obtained by direct simulation, with the largest deviation being $40\ cm^{-1}$ (for the yaw mode of Fe^{2+}).

5. Free Energy Change for Transfer of an Ion from H_2O to D_2O

For an ion with charge $z+$ and n_{HS} water molecules in its hydration shell, all in solvent L_2O, we write the Gibbs function as (cf. text following (4.1))

$$G^{L_2O}(z) = G_{HS}^{L_2O}(z) + G_B^{L_2O}(z)\,. \tag{5.1}$$

The simulation power spectra were used to calculate $\tilde{G}_X^{L_2O}(z)$, the sum of OL stretch and librational contributions of the water molecules to the free energy terms in (5.1). Looking at the set of discrete local modes indexed by m we obtain, for given z,

$$\tilde{G}_X^{L_2O} = n_X \sum_m g_m\, \tilde{G}_{m,X}^{L_2O}\,, \tag{5.2}$$

where g_m is the number of modes of index m. If N is the total number of water molecules in the MD cell, then $n_B = N - n_{HS}$ (here $N = 100$ and $n_{HS} = 6$). The free energy in (5.2) is given by

$$\beta \tilde{G}_m \cong \beta A_m = -\ln q_m\,, \tag{5.3}$$

Table 4. Vibrational zero point contribution to the solvation free energy [a].

Solute	Solvent	Discrete [b]					Cont. [c]
		$\tilde{G}_{Y,HS}^{L_2O}$	$\tilde{G}_{P,HS}^{L_2O}$	$\tilde{G}_{R,HS}^{L_2O}$	$\tilde{G}_{S,HS}^{L_2O}$	$\sum_m \tilde{G}_{m,HS}^{L_2O}$	$\tilde{G}_{HS}^{L_2O}$
Fe^{3+}	H_2O	9.5	11.6	7.7	79.5	108.3	130.5
Fe^{3+}	D_2O	6.8	8.3	5.1	58.9	79.1	90.1
Fe^{2+}	H_2O	8.7	10.2	6.3	82.9	108.1	118.6
Fe^{2+}	D_2O	6.8	7.8	4.9	60.6	80.1	78.1
Fe^{3+}	D_2O [d]	6.9	8.7	5.5	58.2	79.4	
Fe^{2+}	D_2O [d]	6.3	7.7	4.5	60.6	79.1	

[a] In units of RT at 322 K.
[b] For the discrete modes, Y = Yaw, P = Pitch, R = Roll and S = Stretch.
[c] Calculated by (5.5).
[d] Scaled from H_2O data using (4.9).

where $\beta = 1/k_B T$, q_m is the vibrational partition function and we neglect the difference between the Gibbs and Helmholtz free energy. Given the magnitudes of the frequencies in Table 3, we find that for the purpose of calculating differential solvation energies as discussed below, the free energy can be approximated by the zero point expression

$$\beta \tilde{G}_m \cong \tfrac{1}{2}\, \beta \hbar\, \bar{\omega}_m\,, \tag{5.4}$$

where we use $\bar{\omega}_m$ as an estimate of ω_m (cf. (4.8)). As an alternative to (5.2), one may consider the analogous continuous form

$$\tilde{G}_X^{L_2O} = \frac{n_X \int_0^\infty g_X(\omega)\, \tilde{G}_X^{L_2O}(\omega)\, d\omega}{\int_0^\infty g_X(\omega)\, d\omega} \tag{5.5}$$

with $g_X(\omega) / \int_0^\infty g_X(\omega)\, d\omega$ approximated by $P_X^{L_2O}(\omega)$, the normalized L-atom power spectrum (6 modes per water molecule), and with $\tilde{G}_X^{L_2O} = \frac{1}{2}\hbar\omega$.

We apply (5.2) and (5.5) to calculate the vibrational contribution of each mode of the hydration shell to the individual solvation free energies (Table 4). We combine these data to calculate the zero point contribution to $\delta\Delta G$, the difference in ΔG_{trans} (cf. (1.1)) respectively for Fe^{3+} and Fe^{2+}, and thus the change in Gibbs function for the process at 322 K

$$Fe^{3+}(H_2O) + Fe^{2+}(D_2O) \rightarrow Fe^{3+}(D_2O) + Fe^{2+}(H_2O)\,. \tag{5.6}$$

We find $\delta\Delta G/RT = -1.2 \pm 0.5$ from (5.2). If we replace the directly observed D_2O frequencies by the scaled D_2O frequencies from (4.9), we find $\delta\Delta G/$

$RT = -0.1 \pm 0.5$. The same value is derived from the continuous distribution analysis in (5.5).

Notice that we obtain $\delta\Delta G$ as a second difference involving cancellation of relatively large quantities because the separate librational and OL stretch contributions to $\Delta\delta G$ are at least of factor 2 greater than the net value. We may consider these results to be in satisfactory agreement with each other and in only marginally poorer agreement with the following experimental data. Thermocell measurements by Weaver and Nettles [24] give $\delta\Delta G/RT = 1.67$. Also we note NMR shift measurements [25] of the H/D fractionation leading to $\Delta G_{\text{trans}}/RT = 1.88$ and 0.29 for Fe^{3+} and Fe^{2+}, respectively, so the NMR data lead to $\delta\Delta G/RT = 1.59$. Finally, we notice that if in our calculation we neglect the libration terms in Table 4 we would find $\delta\Delta G/RT = 1.7$, in better apparent agreement with experiment.

We conclude that a possible interpretation of the present results is that our models give exaggerated librational contributions to $\delta\Delta G$. There do not seem to be any other data to support this view. It seems more likely that the cause of our low (or negative) $\delta\Delta G$ values is that the present model underestimates the reduction in OH stretch frequency in $M(H_2O)_6^{z+}$ when we change from Fe^{2+} to Fe^{3+}. According to the quantum chemical calculations [3] a decrease of more than 440 cm^{-1} is expected while the data in Table 3 show only a 100 cm^{-1} decrease. The same quantum chemical calculations give r_{OH} for the hydration shell waters in good agreement with experiment [20]. Therefore we expect that modifying the present model to make it more realistic (i.e. smaller OH stretching frequencies and longer r_{OH} for water molecules in the hydration shell of Fe^{3+}) would result in $\delta\Delta G$ values in better agreement with experiment. As before, we assume we can neglect the contribution to $\delta\Delta G$ from the water outside of the hexaaquo complex.

A point for future study is the contribution of non-hydration shell water molecules to $\delta\Delta G$. While MD simulations of the size considered here are adequate to represent the hydration shell [12], there is uncertainty about the possible contribution to $\delta\Delta G$ from the outer shell water. In order to study these effects, one might consider larger systems.

One inviting modification of the model is to increase the partial changes on the oxygen and hydrogen sites in the water model. These charges were originally fit to the gas phase dipole moment, 1.86 D [14]. It has been estimated that the dipole moment in the liquid state is ≈ 2.8 D [26]. We find that the model we are using gives a dipole moment near 2.0 Debye in the liquid state. This suggests that if the partial charges were increased we would obtain a more realistic model. This change seems likely to increase the red shift of the OH stretch modes, leading to more realistic OH stretching frequencies. It is more difficult to predict how these changes will effect the librations. Using the scaled D_2O librational frequencies from Table 3, and using the stretching frequencies calculated in previous work [3] we find $\delta\Delta G/RT = 2.4$, an improvement compared to the results from the present model. We see that the change is in the proper direction, which bodes well for future work with a revised model. The polarization model of Sprik and Klein [26] indicates another promising approach.

The temperature dependence studies in the present work were limited to what was needed to interpolate or extrapolate the simulation data to one temperature. More studies are needed to see whether the present model is consistent with the enthalpy-entropy compensation mentioned in connection with (1.1).

6. Conclusion

Three features of the present study: the model for the water-water and ion-water pair potentials, the MD simulation used to calculate the desired averages for the model system, and the approximations employed to estimate the contribution of the hydration shell to the solvent isotope effect on the Fe^{2+} and Fe^{3+} hydration free energies, all seem quite satisfactory on the basis of the $\delta\Delta G$ results, although some limitations of the model potential have been noticed. The conclusions from earlier quantum chemical calculations that librational modes in the hydration complex are blue shifted by the metal ion while the OL stretch modes are red shifted are confirmed by the present studies, as is the corollary that librational modes and OL stretch modes tend to make mutually cancelling contributions to the solvent isotope effect on the hydration free energies of ions. There is reason from several independent sources to believe that certain defects that have been identified in the water and ion-water model potentials are responsible for some of the discrepancies in the model results, so it is inviting to consider extending the studies to other models in the hope of getting a still better basis for estimating the kinetic isotope effect on the Fe^{2+}, Fe^{3+} electron exchange in aqueous media.

Acknowledgements

This research was carried out in part at Brookhaven National Laboratory under contract DE-AC02-76CH00016 with the U.S. Department of Energy and supported by its Division of Chemical Sciences, Office of Basic Energy. The work at Stony Brook was supported by the National Science Foundation. We also thank Prof. H. G. Hertz for permission to cite unpublished data from his laboratory.

7. Appendix

We calculate the moments of inertia for mode m in L_2O from

$$I_m^L(z+)=\sum_{\alpha=H_1,H_2,O} m_\alpha(\boldsymbol{r}_\alpha(z+)-(\boldsymbol{r}_\alpha(z+)\cdot\hat{A})\,\hat{A})^2, \quad (7.1)$$

where $\hat{A}=\hat{Y}$, $\hat{P}$, or $\hat{R}$ and $\boldsymbol{r}_\alpha=\boldsymbol{r}_{L_1}$, $\boldsymbol{r}_{L_2}$, and $\boldsymbol{r}_O$ are the vectors from the center of mass to the sites in the molecule. Using (7.1) with $|r_{H_1}(3+)|=|r_{H_2}(3+)|=1.0$ Å and $\sphericalangle HOH=100.8°$ we find the folllowing values for the moments of inertia

$$I_Y^D(3+)=3.674941\ \frac{\text{g Å}^2}{\text{mole}},$$

$$I_Y^H(3+)=1.924603\ \frac{\text{g Å}^2}{\text{mole}}, \quad (7.2)$$

$$I_P^D(3+)=1.300180\ \frac{\text{g Å}^2}{\text{mole}},$$

$$I_P^H(3+)=0.727759\ \frac{\text{g Å}^2}{\text{mole}}, \quad (7.3)$$

$$I_R^D(3+)=2.374761\ \frac{\text{g Å}^2}{\text{mole}},$$

$$I_R^H(3+)=1.196844\ \frac{\text{g Å}^2}{\text{mole}}, \quad (7.4)$$

$$\sqrt{\frac{I_Y^H(3+)}{I_Y^D(3+)}}=0.723678, \quad \sqrt{\frac{I_P^H(3+)}{I_P^D(3+)}}=0.748156,$$

$$\sqrt{\frac{I_R^H(3+)}{I_R^D(3+)}}=0.709919. \quad (7.5)$$

[1] J. Bigeleisen, J. Chem. Phys. **32,** 1583 (1959).
[2] J. D. Bernal and G. Tamm, Nature **135,** 229 (1935).
[3] M. D. Newton and H. L. Friedman, J. Chem. Phys. **83,** 5210 (1985).
[4] H. L. Friedman and M. D. Newton, J. Analytical and Interfacial Electrochem. **204,** 21 (1986).
[5] W. J. Albery, Faraday Disc. Chem. Soc. **74,** 111 (1982).
[6] H. L. Friedman and C. V. Krishnan, in: Water: A Comprehensive Treatise (F. Franks, ed.), Vol. 3, Plenum Press, New York 1973.
[7] R. Lumry and S. Rajendar, Biopolymers **9,** 1125 (1970).
[8] R. A. Kuharsaki and P. J. Rossky, Chem. Phys. Lett. **103,** 357 (1984); J. Chem. Phys. **82,** 5169 (1985).
[9] P. J. Adams and G. S. Dubey, J. Comp. Phys. **72,** 156 (1987).
[10] P. Bopp, W. Dietz, and K. Heinzinger, Z. Naturforsch. **34a,** 1424 (1979).
[11] L. A. Curtiss, J. W. Halley, J. Hautman, and A. Rahman, J. Chem. Phys. **86,** 2319 (1987).
[12] S. Engström, B. Jönsson, and R. W. Impey, J. Chem. Phys. **80,** 5481 (1984).
[13] P. Bopp,. G. Jancsó, and K. Heinzinger, Chem. Phys. Lett. **98,** 129 (1983).
[14] A. Rahman and F. H. Stillinger, J. Chem. Phys. **68,** 666 (1978).
[15] G. P. Carney, L. A. Curtiss, and S. A. Langhoff, J. Mol. Spect. **61,** 371 (1976).
[16] L. Verlet, Phys. Rev. **159,** 98 (1967).
[17] J. E. Enderby, S. Cummings, G. J. Herdman, G. W. Neilson, P. S. Salmon, and N. Skipper, J. Phys. Chem. **91,** 5851 (1987). – G. W. Neilson and J. E. Enderby, Proc. Roy. Soc. London **A 390,** 353 (1983).
[18] R. D. Shannon and C. T. Prewitt, Acta Crys. **B 25,** 938 (1969).
[19] A. K. Soper, G. W. Neilson, J. E. Enderby, and R. A. Howe, J. Phys. C **10,** 1793 (1977). – D. R. Sandstrom and F. W. Lytle, Ann. Rev. Phys. Chem. **30,** 215 (1979). – J. P. Hunt and H. L. Friedman, Progress in Inorganic Chem. **30,** 359 (1983).
[20] J. R. C. van der Maarel, H. R. W. M. de Boer, J. de Bleijser, D. Bedeaux, and J. C. Leyte, J. Chem. Phys. **86,** 3373 (1987).
[21] R. P. Futrelle and D. J. McGinty, Chem. Phys. Lett. **12,** 285 (1971).
[22] J. W. Halley and J. Hautman, Ber. Bunsenges. Phys. Chem. **91,** 491 (1987).
[23] I. Nakagawa and T. Shimanouchi, Spectrochimica Acta **20,** 429 (1964).
[24] M. J. Weaver and S. J. Nettles, Inorg. Chem. **19,** 1641 (1980).
[25] H. G. Hertz, private communication.
[26] M. Sprik and M. L. Klein, J. Chem. Phys. **89,** 7556 (1988).